Proceedings of Global Power and Propulsion Society
ISSN-Nr: 2504-4400
GPPS Montreal26
September 9-11, 2026
www.gpps.global

GPPS-TC-2026-0186

INVESTIGATION OF ROTOR-STATOR INTERACTION NOISE IN A DUCTED ROTOR CONFIGURATION

Ralph Kinte Pouhe Hiol
École de Technologie Supérieure
ralph-kinte.pouhe-hiol.1@ens.etsmtl.ca
Montréal, QC, Canada

Marlène Sanjosé
École de Technologie Supérieure
marlene.sanjose@etsmtl.ca
Montréal, QC, Canada

Jose Rendón-Arredondo
Université de Sherbrooke
jose.manuel.rendon.arredondo@usherbrooke.ca
Sherbrooke, QC, Canada

ABSTRACT

Rotor-Stator Interaction (RSI) noise is investigated in a ducted tail rotor configuration to assess the capability of low-fidelity approaches to accurately predict the associated tonal and broadband levels. The methodology couples Reynolds Averaged Navier-Stokes (RANS) simulations performed on a restricted 180° periodic domain for aerodynamic quantities with semi-analytical models for far-field noise evaluation. Particular attention is paid to the rotor wake and the tip leakage vortex (TLV) excitations on the stator vanes, which constitute the main RSI noise sources. The model-based predictions are compared with reference far-field noise obtained from the Lattice Boltzmann Method (LBM) combined with the solid formulation of the Ffowcs Williams and Hawkings (FW-H) acoustic analogy. Good agreement is observed between RANS and LBM regarding the velocity distribution in the interstage region. Despite some discrepancies observed in acoustic predictions, especially regarding tonal levels, the low-fidelity approach allows for the ranking of noise mechanisms, supporting manufacturers in making decisions about their designs.

INTRODUCTION

Increasing concerns within the community regarding environmental issues and noise pollution have led to the adoption of more stringent regulations for the design of new rotorcraft (Organization, ICAO). Among the various sources of noise in turbomachinery, aerodynamic noise remains a primary concern in aircraft design. Ducted rotor configurations have gained particular interest over recent decades within the turbomachinery community. In addition to enhancing the safety of people operating near these systems, they have shown to improve aerodynamic performance compared to equivalent open configurations. Recent studies have also shown promising noise mitigation capabilities (Malgoezar et al., 2019). They are usually associated with stator vanes that straighten the flow downstream the rotor, leading to an improvement of the overall performance of the machine. However, this gain in performance comes with an additional noise source, the Rotor-Stator Interaction (RSI) noise, which arises from the interaction of the vortical structures downstream of the rotor row, the wake and tip leakage vortex (TLV), with the leading edge of the stator vanes. According to Glegg and Devenport (2017), this mechanism is the dominant noise source in modern turbofans.

RSI noise can be accurately predicted using high-fidelity simulations coupled with acoustic analogy (Moreau, 2022). However, in an industrial context, especially during the design process, this approach is difficult to implement due to the complexity of the configurations involved and the associated computational cost. Therefore, low-to-mid fidelity simulations coupled with semi-analytical models appear to be a more practical alternative for noise prediction. The semi-analytical models rely on the decomposition of the noise emission process into several phases: the aerodynamic excitation, the blade surface response to that excitation, and the far-field propagation (Moreau and Roger, 2024). Most of the models in the literature only account for the perturbations arising from the rotor wake, neglecting the specific dynamics of the TLV that can be significant in short duct configurations.

This study aims to assess the capability of RANS simulations coupled with semi-analytical models for the prediction of RSI noise. To this end, investigations are performed on a ducted rotor configuration made up of 4 rotor blades and 6 stator

This work is licensed under **Attribution-NonCommercial-NoDerivatives 4.0 International (CC-BY-NC-ND)**
See: https://creativecommons.org/licenses/by-nc-nd/4.0/legalcode

vanes. The Reynolds number based on the chord is $Re_c = 4.5 \times 10^5$ and the mach number at the tip is 0.42. The paper is organized as follows. The configuration under study, the numerical simulation and acoustic methods are first presented in the methodology section. The results section provides a description of the aerodynamic fields in the investigated configuration and details the aerodynamic excitation obtained in the RANS simulation. The acoustic predictions are discussed with respect to a reference high-fidelity simulation performed with an LBM approach.

METHODOLOGY

This section provides the numerical parameters used for RANS simulations and the acoustic computation of the far-field noise associated with the RSI mechanism.

Computational domain and grid

The computational domain shown in Fig. 1 is divided into 2 regions separated by an interface. A rotating domain encompasses the inlet and the rotor assembly composed of 2 rotor blades, the rotor hub, and a section of the fan duct (shown in green). The stationary domain contains 3 stator vanes (shown in blue) and the outlet. Since only a 180° angular sector of the fan is simulated, periodic boundary conditions are used in both regions. The domain is discretized using an unstructured

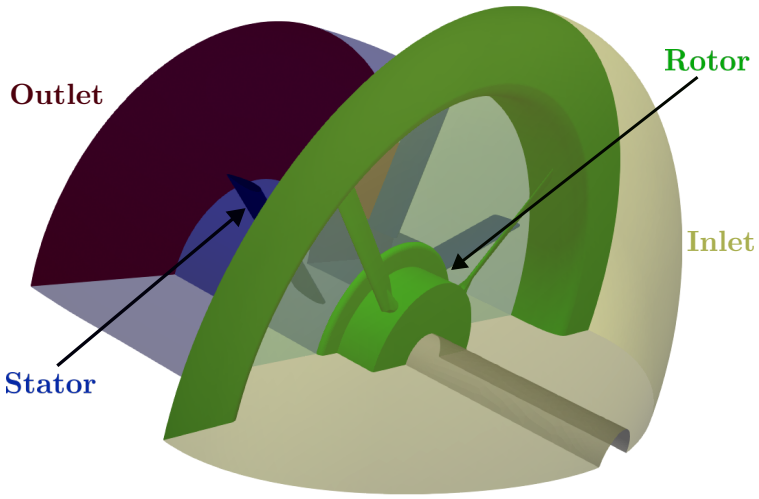


Figure 1 Computational domain for RANS simulations

hybrid mesh, generated with CENTAUR software V18.5, composed of 81 million prismatic cells in the near-wall regions around the blade, vane, and casing surfaces, and 188 million tetrahedral cells in the rest of the domain. The boundary layer at the wall surfaces is discretized using 17, 15, and 10 cells in the prismatic layer, respectively, with a stretching ratio of 1.25. Near-wall cells have an aspect ratio of about 200 on the blade surfaces, and 100 on both the vanes and the casing. These parameters lead to mean y^+ values around 4.82 on the blade and 1.62 and 3.0 on the vane and the casing respectively. The mesh characteristics are summarized in Table 1.

Surface	y^+_{mean}	Aspect ratio	Stretching ratio	n_{layers}
Blade	4.82	200	1.25	17
Vane	1.62	100	1.25	15
Casing	3.0	100	1.25	10

Table 1 Mesh characteristics in near-wall region

Another computational domain, consisting of only 1 rotor blade without stator vanes, is used in this study to extract flow quantities after the interface. These simulations will be labeled as RANS-RS for the rotor/stator and RANS-RO for the rotor only configurations.

Numerical simulation method

Compressible RANS simulations are performed with the commercial solver ANSYS CFX 2024.R1. Turbulence is accounted for using the $k-\omega$ SST closure model (Menter, 1994) coupled with the $\gamma - Re_\theta$ model (Menter et al., 2004) to handle transition. Convective terms of the averaged N-S equations are discretized using the High resolution scheme, available in Ansys CFX, which can be of first or second order accuracy depending on local gradients in the solution. A constant mass flow rate, corresponding to the fan hovering conditions estimated at design, is imposed at the inlet, while

a reference static pressure is imposed at the outlet. Surfaces are set as adiabatic no-slip walls, except for the shaft, where a free slip wall boundary condition is imposed. The interface connecting the rotating and stationary domains is modelled using a mixing plane approach in which circumferential averaging of flow quantities is performed. The static pressure is assumed to be continuous across the interface while the downstream velocity field is reconstructed from the circumferential average of total pressure (ANSYS, Inc, 2022).

Acoustic method

The far-field noise is calculated using a set of analytical models to represent the various noise mechanisms. Two main excitations for the RSI are considered in the present study: the downstream rotor wake and the tip leakage vortex. The resulting far-field noise can be decomposed into tonal and broadband noise contributions. The tonal components arise from the periodic impingement of the rotor wakes and tip leakage vortex. The broadband noise is associated with the turbulent content carried by these secondary flow features.

The tonal noise generated by the periodic impingement of the rotor wakes on the stator vanes is computed using the Goldstein analogy, which relates the far-field acoustic power in both upstream and downstream directions to the unsteady lift response of the vane surfaces to an incoming perturbation (Goldstein, 1976; Pestana, 2020). This response is obtained using the Amiet-based Schwarzschild approach (Amiet, 1975) applied to a Fourier decomposition of the upwash velocity field. The tonal noise contribution from the tip leakage vortex is evaluated following the methodology proposed by Quaglia et al. (2017) and originally developed for Orthogonal Blade-Vortex Interaction (OBVI) in Counter-Rotating Open Rotor (CROR). It consists of extracting the tip vortex trajectory, core radius, tangential velocity, and axial velocity deficit at several locations downstream from the rotor and extrapolating the upwash velocity perturbation caused by the TLV right at the vane leading-edge.

The broadband noise component is evaluated using Amiet's theory for leading edge noise (Amiet, 1975). The 2D Von Karman model is used to reconstruct the turbulent upwash velocity spectrum that characterizes the excitation. Trailing edge noise is also evaluated using Amiet's theory (Amiet, 1976). Boundary layer parameters are extracted at 85% of the chord, and the wall-pressure spectrum is reconstructed using Rozenberg's model (Rozenberg et al., 2012).

The objective of the present work is to evaluate this methodology based on RANS informed excitation. For this purpose, results from the Lattice Boltzmann Method (LBM) simulations carried out on the full 360° configuration (Rendon et al., 2024) serve as reference. The numerical methodology for the LBM simulation is thoroughly described by Rendón and Moreau (2025). The acoustic spectra obtained with analytical approach are compared with a Ffowcs Williams and Hawkings (FW-H) analogy integrating the wall-pressure on the stator vanes only. Data have been recorded for more than 10 revolutions.

AERODYNAMIC RESULTS

This section provides a comparison of the main aerodynamic results obtained with the reference data extracted from LBM simulations.

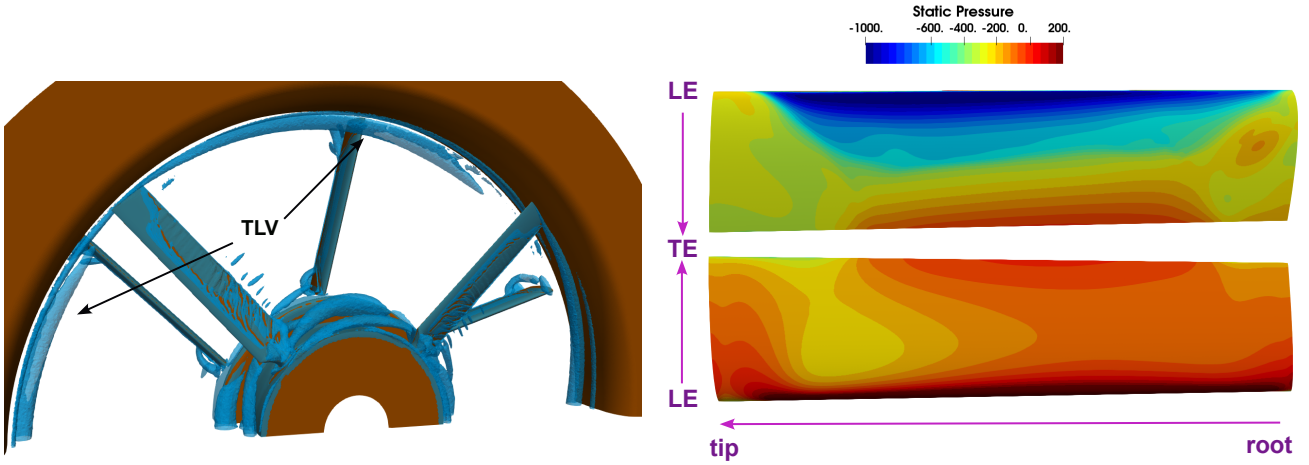
Flow analysis

The iso-surfaces of Q-value for the RANS simulation are shown on the left-hand side in Figure 2a providing a qualitative representation of the secondary flow structures. The region around the hub is affected by the large vortical structures that originate from the blades root and are convected downstream towards the stator hub. Near the casing, the TLV interacts with the developing boundary layer at the casing entrance, but does not remain coherent for more than one blade passage due to the presence of the mixing plane. Figure 2b shows the static pressure distribution on both the suction and pressure sides of the vane. A diagonal trace of low pressure is seen on the pressure side of the vane and might be linked to the TV impingement on the stator. A similar feature was seen by Rendón and Moreau (2025) using high-fidelity simulations.

Figure 3 shows the mean axial velocity and the TKE in the meridional plane, made non dimensional by the rotor tip speed $\Omega\, R_{tip}$, with Ω the rotational speed. The axial velocity contours highlight two low-speed regions. The first is near the root of the blade, where large vortical structures were observed in Fig 2a , and the second is along the casing, consecutive of a boundary flow separation. Both regions exhibit high turbulence intensity levels as evidenced by turbulent kinetic energy (TKE) contours map. Additionally, the tip vortex that originates in the vicinity of the blade gives rise to a high TKE zone that starts from the trailing edge of the rotor and propagates downstream towards the stator vane leading edge.

The axial, radial, and tangential velocity components, along with the TKE, are extracted at two axial positions L1 and L2, in the meridional plane as indicated by the white lines in Figure 3. L1 is positioned $0.1c$ downstream of the rotor blade trailing edge and L2 is located $0.1c$ upstream of stator vane leading edge. RANS and LBM meridional profiles are compared in Figure 4. The non dimensional radius r^* is computed using Eq. (1), with R_{root} and R_{tip} the radial extents of the rotor blades. The horizontal dashed line indicates the radial position of the stator hub. All quantities have been made non dimensional by the linear rotor tip speed ΩR_{tip}.

$$r^* = \frac{r - R_{root}}{R_{tip} - r_{root}} \tag{1}$$



(a) Isosurfaces of Q-criterion in RANS simulations

(b) Static pressure contours on the stator in RANS simulations

Figure 2 Flow visualization quantities

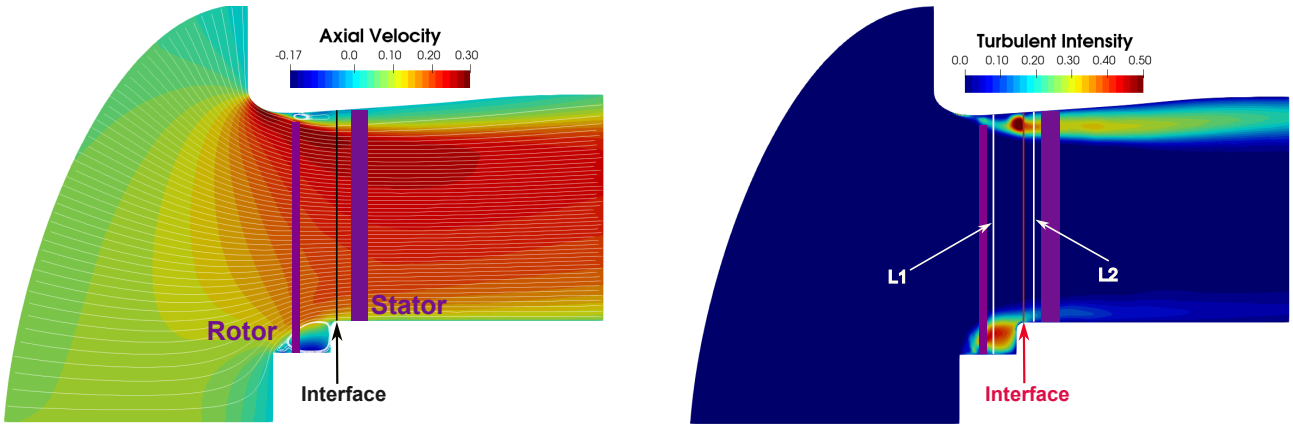


Figure 3 Contours of flow quantities in the meridional plane. *Left:* Axial velocity. *right:* Turbulence Kinetic Energy

Both RANS and LBM yield similar axial and tangential velocity distributions. Flow blockages induced by the recirculation region near the blade root and the TLV are clearly identified by the negative values of the axial and radial velocity in both simulations. The TKE distribution in RANS suggests that the stator leading edge ingests high intensity turbulence in the tip region, coming from the rotor and which can be a major source of noise. Discrepancies are observed with LBM levels, which highlight the same peaks but at much lower amplitudes.

Tip vortex extraction

The coordinates of the tip vortex center are extracted by performing several iso-θ plane cuts starting from the azimuthal position of the preceding blade. On each plane, the vortical structures are isolated in a restricted region by applying a Q-criterion threshold of $5 \times 10^5 s^{-2}$. Then, the vortex core location is identified as the locus of minimum pressure within the vortex. As performed by Quaglia et al. (2017), the coordinates of the vortex core in the cylindrical basis of the machine are modelled with a helix of linearly varying radius following Eq. (2),(3).

$$R_v = \alpha_\beta X_v + R_i \tag{2}$$

$$\theta_v = \beta_\phi X_v + \Phi_i \tag{3}$$

where R_i and ϕ_i are the initial radial and angular positions of the helix in the cylindrical frame, R_v and θ_v are its radial and angular positions along the trajectory, and X_v is the axial coordinate measured from the starting point of the vortex on the preceding blade. α_β is the stream tube contraction coefficient, and β_ϕ is the axial advance of the helix.
Figure 5 shows the radial and angular positions (R_v, θ_v) of the vortex core as a function of its axial position X_v for the complete RANS-RS configuration shown in Figure 1, for RANS-RO and for the LBM simulations. As can be seen on the left-hand side, both RANS simulations give similar radial position R_v until the location of the interface. For the RANS-RS configuration, the extraction is only possible until the rotor stator interface because of the mixing plane. Differences are

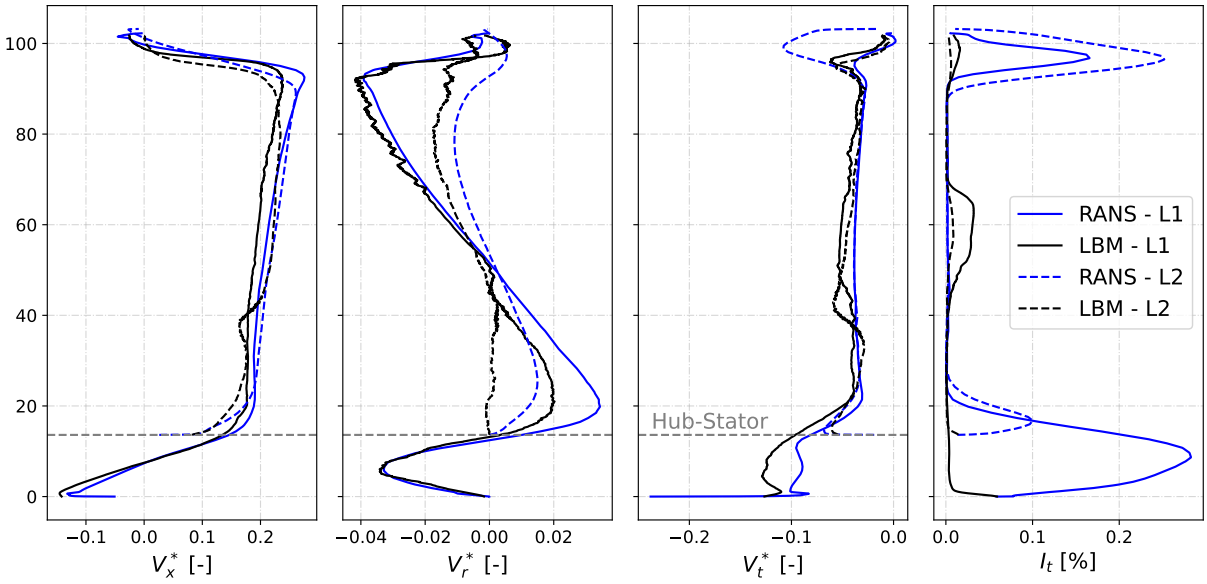


Figure 4 Axial (V_x), radial (V_r) and tangential (V_t) velocity components and Turbulence intensity (I_t) profiles extracted at two axial positions in the meridional plane

observed in the angular position. The lower angle values obtained for the configuration including the stator vanes highlight a portion of swirl which is straightened by the stator row. LBM shows good agreement with RANS-RS in terms of angular position, but discrepancies are observed in the values of the radial coordinate. RANS-RO data are used to extract the vortex properties up to the stator location without relying on extrapolation.

Figure 6 shows the evolution of the dimensionless vortex core radius r_0 and maximal azimuthal velocity as a function of the axial advance X_v. The core radius is defined as the location where the tangential velocity in the reference frame of the vortex is at its maximum. Along the machine axis, r_0 increases and $V_{theta,max}$ decreases, which indicates a roughly conservation of vortex strength.

The velocity profiles in the reference frame of the vortex, at a location just upstream of the stator leading-edge, are extracted within a disk centered on the center of the vortex, averaged over the azimuth, and plotted in Fig 7. The gray area represents the standard deviation around the mean. The extracted azimuthal velocity profile is compared with three analytical models, as shown on the left. The Taylor vortex model better captures the decay in the viscous region of the vortex and is used as input to the upwash reconstruction model. The radial velocity is neglected in the upwash modeling.

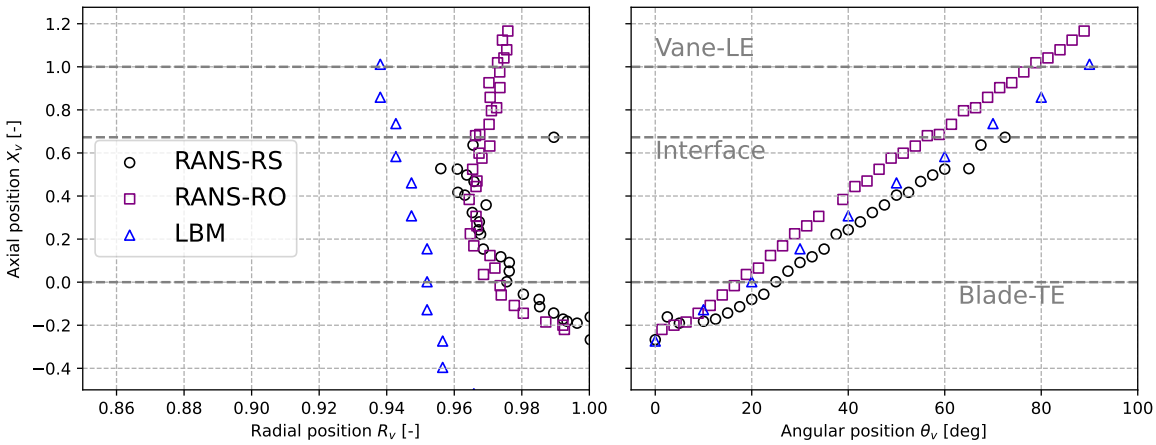


Figure 5 Tip vortex core trajectory in cylindrical coordinates (R_v, θ_v, X_v)

Wake extraction

As outlined in the methodology section, a Fourier decomposition is applied to the upwash velocity field that serves as input for the tonal noise model. The wake is extracted in a plane located $0.1c$ upstream of the interface, ensuring that wake

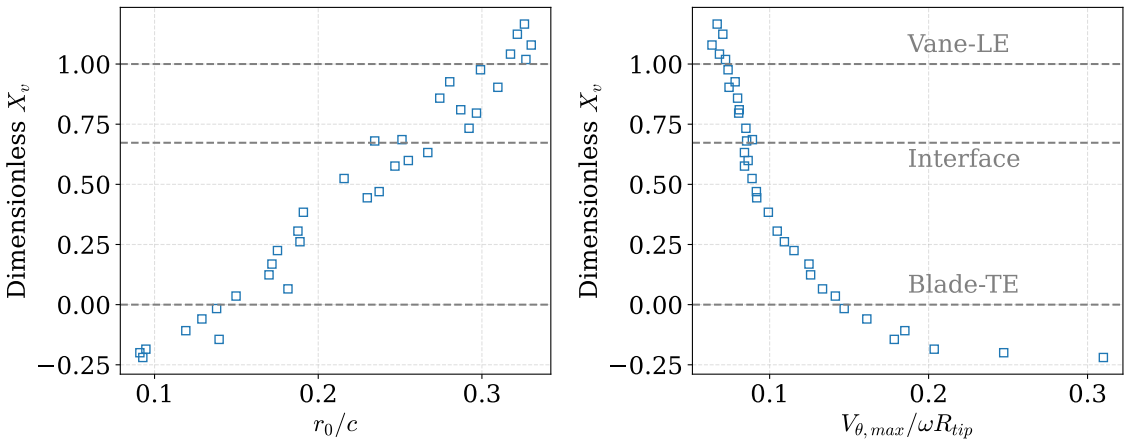


Figure 6 Variations of the dimensionless core radius and maximum azimuthal velocity with the axial position of the center of the vortex

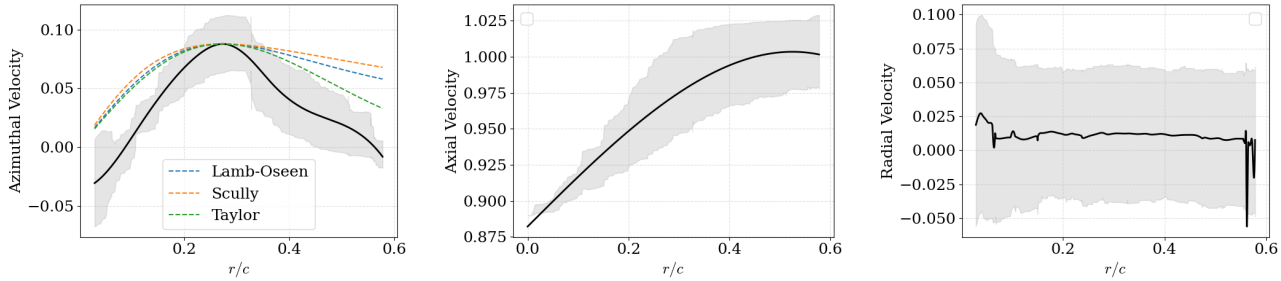


Figure 7 Dimensionless velocity profiles in the reference frame of the vortex upstream of the stator leading-edge.

content is properly captured while avoiding any bias introduced by the averaging process at the interface.
To isolate the perturbation that comes solely from the wake, an azimuthal average of velocity components is performed in a region of radii $r \in [R_v - 1.5r_0,\ R_{duct}]$ of the extraction plane. Figure 8 shows a comparison between filtered and non-filtered upwash velocity in that plane.

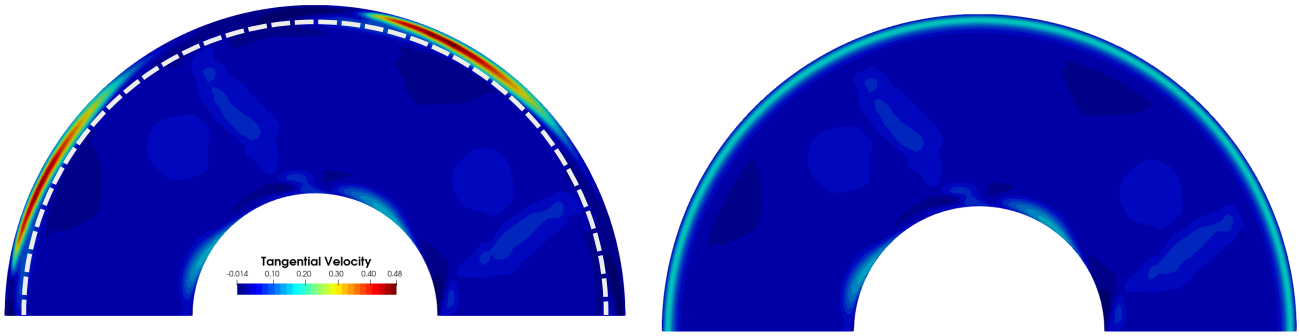


Figure 8 Dimensionless tangential velocity in a plane $0.1c$ upstream of the interface. *Left:* Axial velocity $0.1c$ upstream of the interface. *Right:* TKE $0.1c$ upstream of the stator leading edge

ACOUSTIC RESULTS

This section compares the far-field acoustic spectra obtained using analytical modeling informed from RANS-based inputs with the reference LBM.

Figure 9 shows the sound power level radiated upstream and downstream of the rotor plane. In terms of broadband noise, LBM exhibits almost constant levels within the entire power spectrum. A roll-off is observed at $f/BPF = 30$ and

is related to the sampling frequency on the stator surface. Broadband levels in RANS are lower by about 5-10 dB than those from LBM. Noise source decomposition shows that the trailing edge noise from the stator (in orange) has a negligible contribution compared with the leading edge noise from the stator (in red).

Regarding the tonal noise, RANS-informed analytical models exhibit higher amplitudes than those obtained with LBM. The amplitudes of BPF harmonics in the LBM spectra are integrated to account for the full energy distributed around the peaks due to the limited physical time duration of the simulations.

Figure 10 shows a decomposition of the tonal mechanisms, isolating the acoustic contributions from the rotor wake and the tip leakage vortex. The wake-interaction mechanism, computed using the Goldstein analogy, does not produce noise at the BPF, as it is lower than the duct cut-off frequency. At the BPF, the tip vortex stands as the sole contributor, with a peak amplitude slightly overpredicting the LBM reference. The tip vortex excitation is found to dominate the first three harmonics, whereas the wake excitation dominates at higher harmonics. Overall, good agreement is achieved with LBM despite the overprediction of levels. In particular, the low-fidelity model provides the right trends in terms of tone amplitude compared with the LBM results. Further studies need to be done to ensure the reliability of the acoustic predictions.

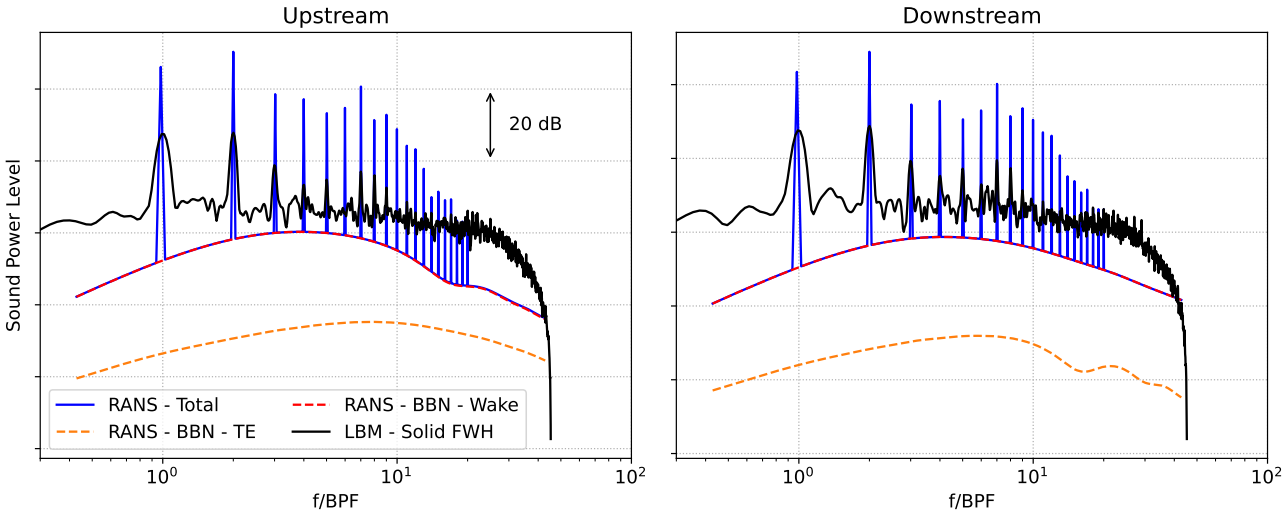


Figure 9 Comparison of acoustic power between RANS and LBM

CONCLUSIONS

Low-fidelity approaches informed by RANS-based inputs have been used to investigate the noise contributions generated by the rotor-stator interactions in a ducted rotor-stator configuration. Two competing noise mechanisms, caused by secondary flow structures produced by the rotor, the wake and the tip-leakage vortex, are analyzed and modelled. The former is modelled as an unsteady loading of the vanes computed using an Amiet response and a Goldstein analogy for in-duct propagation, while the latter is computed as a localized perturbation, and a Hanson-Parzych free-field response is used to capture the orthogonal vortex interaction. First, the extracted flow properties are evaluated. Comparison of the velocity profiles with reference data from high-fidelity Lattice Boltzmann Method (LBM) simulations shows good agreement, but some differences have been observed in terms of TKE levels. Regarding the noise, RANS informed analytical models overestimate tones and underestimate the broadband components compared with LBM reference spectra. Despite some inaccuracies, the use of low-fidelity approaches allows for the identification of main noise mechanisms. For this configuration, the main broadband contribution comes from the turbulent ingestion noise at the leading-edge due to rotor wake impingement, rather than the trailing-edge noise. The tip-vortex interaction is dominant at low harmonics, while the wake interaction becomes dominant at the 4th BPF harmonics.

Further studies could be dedicated to the use of more elaborate models accounting for spanwise correlation effects and broadband contributions from the tip vortex.

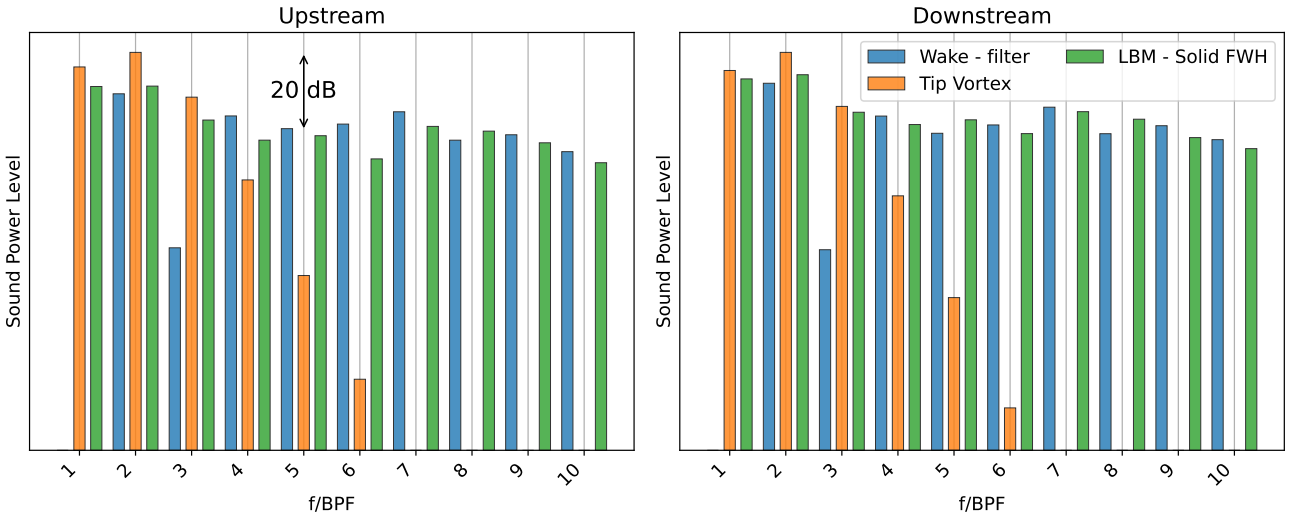


Figure 10 Comparison of tonal levels for the first 10 harmonics

ACKNOWLEDGMENTS

This work was conducted as part of research project ALLRP-570863-21 funded by NSERC and Mitacs with contributions from Bell Textron Canada Limited and Optis Consultants Inc. The low-fidelity simulations were performed using OptiSound, developed and distributed by Optis. The simulations and their analysis were performed on the Trillium supercomputers operated by SciNet and managed by the Digital Research Alliance of Canada. Post-processing was enabled in part by means of the Antares Python API developed by CERFACS.

REFERENCES

Amiet, R. (1975), 'Acoustic radiation from an airfoil in a turbulent stream', *Journal of Sound and Vibration* **41(4)**, 407–420.

Amiet, R. (1976), 'Noise due to turbulent flow past a trailing edge', *Journal of Sound and Vibration* **47**(3), 387–393.

ANSYS, Inc (2022), CFX-Solver Modeling Guide, Documentation 2022.R2, Canonsburg, PA.

Glegg, S. and Devenport, W. (2017), *Aeroacoustics of Low Mach Number Flows: Fundamentals, Analysis, and Measurement*, Vol. 1, Academic Press.

Goldstein, M. E. (1976), *Aeroacoustics*, McGraw-Hill International Book Co, New York.

Malgoezar, A. M., Vieira, A., Snellen, M., Simons, D. G. and Veldhuis, L. L. (2019), 'Experimental characterization of noise radiation from a ducted propeller of an unmanned aerial vehicle', *International Journal of Aeroacoustics* **18**(4-5), 372–391.

Menter, F. R. (1994), 'Two-equation eddy-viscosity turbulence models for engineering applications', *AIAA Journal* **32**(8), 1598–1605.

Menter, F. R., Langtry, R. B., Likki, S. R., Suzen, Y. B., Huang, P. G. and Völker, S. (2004), 'A Correlation-Based Transition Model Using Local Variables—Part I: Model Formulation', *Journal of Turbomachinery* pp. 413–422.

Moreau, S. (2022), 'The third golden age of aeroacoustics', *Physics of Fluids* **34**(3), 031301.

Moreau, S. and Roger, M. (2024), 'Turbomachinery Noise Review', *International Journal of Turbomachinery, Propulsion and Power* **9**(1), 11.

Organization(ICAO), I. C. A. (2017), Annex 16 to the Convention on International Civil Aviation : Environmental Protection - Volume I : Aircraft Noise, Technical report, ICAO; Montréal, Québec, Canada.

Pestana, M. (2020), Effets d'un Stator Hétérogène Sur Le Bruit d'interaction Rotor-Stator : Étude Analytique, Expérimentale et Numérique, PhD thesis, Ecole Centrale de Lyon.

Quaglia, M. E., Léonard, T., Moreau, S. and Roger, M. (2017), 'A 3D analytical model for orthogonal blade-vortex interaction noise', *Journal of Sound and Vibration* **399**, 104–123.

Rendón, J. and Moreau, S. (2025), On the effect of tip flow on the noise of a ducted rotor, *in* 'International Conference on Fan Noise, Aerodynamics, Applications and Systems', Antibes, Juan-les-Pins, France.

Rendon, J., Moreau, S. and Sanjosé, M. (2024), 'Influence of the rotor blade pitch angle on the far-field noise emissions of a ducted tail rotor', *Proceedings of the 30th AIAA/CEAS Aeroacoustics Conference* **AIAA 2024-3150**.

Rozenberg, Y., Robert, G. and Moreau, S. (2012), 'Wall-Pressure Spectral Model Including the Adverse Pressure Gradient Effects', *AIAA Journal* **50**(10), 2168–2179.